



# Crossed polarization optical transmittance spectra as a way of determining wing thickness of the *Episcada Hymenaea* translucent butterfly

Juan P. Martínez<sup>1</sup> · Pablo Fagúndez<sup>2</sup> · C. Javier Pereyra<sup>1</sup> · Mariana Pereyra<sup>2</sup> · Gabriela Bentancur-Viglione<sup>3</sup> · Enrique Morelli<sup>3</sup> · Paulo Valente<sup>1</sup> · Ricardo E. Marotti<sup>1</sup>

Received: 3 June 2023 / Accepted: 9 July 2023  
© The Author(s), under exclusive licence to The Materials Research Society 2023

## Abstract

The accurate determination of sample thickness is crucial for its comprehensive characterization in materials science. Interference oscillations in optical spectra offer a simple method to achieve this, relying on the sample's preservation of light coherence. However, conventional spectra may fail to exhibit these oscillations in numerous samples due to factors such as high transparency, anisotropy, or scattering caused by nanostructures. In this study, we implement a crossed polarization spectral transmittance measurement which successfully unveils hidden interference oscillations by exploiting the polarization conversion characteristics in the wing of the *Episcada hymenaea* translucent butterfly. We compare the thickness measurements obtained using this method with those derived from Scanning Electron Microscopy and find a relative difference as low as 5% as well as high robustness against variations in the refractive index.

## Introduction

The fascinating properties exhibited by various materials found in nature often surpass expectations based on their constituent components, a phenomenon that is frequently attributed to intricate hierarchical nanostructures [1, 2]. In recent decades, biomimetics [3] and bio-inspired materials have witnessed substantial progress, yielding advancements in properties such as tensile strength [4], hydrophobicity [2, 5], and drag reduction [3]. Within this realm, structural color has emerged as a topic of growing interest, owing to

its potential for mitigating pollution by reducing the use of contaminating dyes [6, 7]. Of particular significance is the investigation of structural color in butterfly wings, with the *blue morpho* butterfly serving as a paradigmatic example [8, 9], while other species have shown fascinating polarization sensitive color properties [10–13].

While the optical properties of butterfly wings have been extensively studied, recent developments have harnessed their anisotropy for various technological applications. Butterfly wings have been employed as vapor detectors [14], thermal sensors [15], and platforms for Surface Enhanced

✉ Juan P. Martínez  
jmartinez@fing.edu.uy  
Pablo Fagúndez  
pfagundez@fcien.edu.uy  
C. Javier Pereyra  
jpereyra@fing.edu.uy  
Mariana Pereyra  
mpereyra.perez@fcien.edu.uy  
Gabriela Bentancur-Viglione  
gbentancur@fcien.edu.uy  
Enrique Morelli  
emorelli@fcien.edu.uy  
Paulo Valente  
pvalente@fing.edu.uy

Ricardo E. Marotti  
khamul@fing.edu.uy

<sup>1</sup> Facultad de Ingeniería, Instituto de Física, Universidad de la República, Julio Herrera y Reissig 565, 11300 Montevideo, Montevideo, Uruguay  
<sup>2</sup> Facultad de Ciencias, Unidad de Bioquímica Analítica, Universidad de la República, Iguá 4225, 11400 Montevideo, Montevideo, Uruguay  
<sup>3</sup> Facultad de Ciencias, Sección Entomología, Universidad de la República, Iguá 4225, 11400 Montevideo, Montevideo, Uruguay

Raman Spectroscopy (SERS) [16]. In understanding and optimizing these applications, accurate knowledge of wing thickness is crucial, as it directly influences optical and mechanical performance, and often serves as a prerequisite for determining other parameters, such as the refractive index. Currently available techniques for measuring thickness, such as ellipsometry [17] and interferometry [18], are very reliable but possess certain limitations, including their specialized nature and high cost.

To address these challenges, we propose a straightforward technique to determine the thickness of *Episcada hymenaea* translucent butterfly wings based on interference oscillations in the spectral transmittance aided by polarization conversion. This species is particularly intriguing due to its similarity with the *Greta oto* [19, 20], which exhibits remarkably low reflectance over a wide range of incident angles. Notably, both species are one of the few examples of transparency-based camouflage found in terrestrial environments. The transparency of the wings presents a unique challenge, as the oscillations required for thickness calculations are not readily discernible in the direct spectra. To overcome this limitation, we have implemented a novel crossed polarization measurement approach that effectively exploits the anisotropy within the nanoscale structure. This technique significantly enhances contrast and unveils the oscillations necessary for precise thickness determination, employing only linear polarizers.

## Materials and methods

The transmittance measurements were performed with a halogen lamp, model HL-2000 from Ocean Optics as the light source. The lamp was connected to a collimator by a 1000  $\mu\text{m}$  optical fiber to focus the light onto the sample, which was mounted on a goniometer. To confine the analysis to the transparent portion of the wing and minimize the influence of the sample holder, two irises were positioned

in the incoming path, effectively reducing the spot size. The transmitted light was collected using another collimator and detected with a fiber-coupled spectrometer, namely the S2000 model from Ocean Optics. The sample holder, an aluminum plate with a centrally positioned hole, was placed between a polarizer and an analyzer. The wing was clamped at the bottom of the plate, allowing most of the structure to remain unobstructed above the hole, where the light was incident. For a schematic of the setup, see Fig. 1a.

For the transmittance measurements, different polarizer–analyzer configurations, denoted as  $T_{ij}$ , ( $i, j = 1, 2$ ), were employed. The first index represents the position of the polarizer, while the second index corresponds to the position of the analyzer. To establish an orthonormal basis for polarization, the following procedure was implemented without placing a sample in the sample holder (lamp signal only):

1. The polarizer was set at an arbitrary angle, defining the  $i = 1$  position.
2. The analyzer was rotated until the signal was maximized, determining the  $j = 1$  position.
3. The analyzer was rotated again until the signal was minimized, establishing the  $j = 2$  position.
4. With the analyzer in the second position ( $j = 2$ ), the polarizer was rotated until the signal was maximized once more, representing the  $i = 2$  position.

Consequently, four configurations were obtained:  $T_{11}$  and  $T_{22}$  for parallel (or direct) transmitted light and  $T_{12}$  and  $T_{21}$  for crossed-polarized transmittance. The crossed polarization signals were normalized to the direct polarization measurement without the presence of a sample, using the configuration that matched the first index. For instance,  $T_{12}$  was normalized with respect to  $T_{11}$ . To calibrate normal incidence ( $\phi_i = 0^\circ$ ), a glass plate was placed on the sample holder, and its position was adjusted until the reflection aligned with the incoming beam.

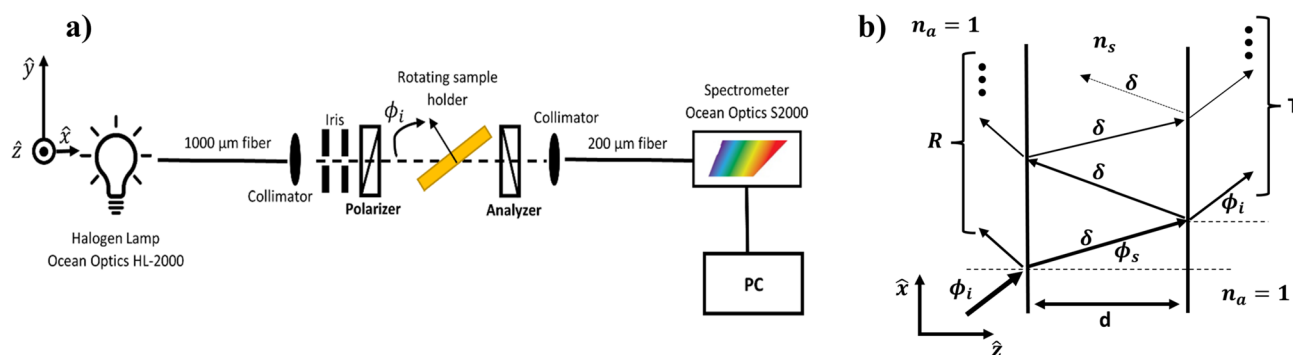


**Fig. 1** **a** Experimental setup used to measure spectral cross-polarized transmittance and **b** Schematic of the model used to calculate the transmittance of a thin film

To evaluate the suitability of the technique, a comparative analysis is conducted, whereby the thickness derived from the experimental spectra is contrasted against measurements obtained through imaging with a scanning electron microscope (SEM), model JSM/5900 LV SEM from JEOL.

### Interference in thin films

To calculate the thickness ( $d$ ) of the wing based on the transmittance spectra, we employed the formula for an isotropic and homogeneous thin film [21]. Considering the situation depicted in Fig. 1b, where a single unsupported layer is embedded in air, we see that the overall transmission ( $t$ ) is a superposition of an infinite number of beams, each following a different path through the sample. The total transmission ( $t$ ) is given in Eq. 1.

$$t = t_{as} e^{i\delta} t_{sa} [1 + r_{sa}^2 e^{2i\delta} + (r_{sa}^2 e^{2i\delta})^2 + \dots]. \tag{1}$$

Equation 1 introduces the Fresnel transmission (reflection,  $r$ ) coefficients for light passing through an air-sample interface. The coefficients  $t_{as}$  ( $r_{as}$ ) represent the transmission (reflection) coefficients of light when it approaches the interface from air. Conversely, the coefficients  $t_{sa}$  ( $r_{sa}$ ) correspond to the case of light approaching the interface from the sample. Meanwhile,  $\delta$  is the optical path length traversed through the sample. As  $|r_{sa}^2 e^{2i\delta}| < 1$  the geometric series converges to the result in Eq. 2.

$$t = \frac{t_{as} t_{sa} e^{i\delta}}{1 - r_{sa}^2 e^{2i\delta}}, \tag{2}$$

$$\delta = 2\pi \nu d \sqrt{\hat{n}_s^2 - \sin^2 \phi_i}. \tag{3}$$

The optical path  $\delta$  traveled by a wave through the sample can be expressed as shown Eq. 3 by using Snell's law [21], where  $\nu = \frac{1}{\lambda}$  is the wave number,  $d$  is the sample thickness,  $\phi_i$  is the angle of incidence, and  $\hat{n}_s$  is the (possibly complex) refractive index of the sample.

The transmission coefficient represents the fraction of incoming amplitude that is transmitted. Since our measured quantity is intensity, the transmittance  $T$  is the relevant parameter. It is defined as  $T = |t|^2$  in cases where the incoming and exit media are the same [21]. In the particular case of vanishing damping  $\hat{n}_s$ ,  $r_{sa}$ , and  $\delta$  are real, and the transmittance ( $T$ ) is expressed using Eq. 4. If the refractive index, and thus, the Fresnel coefficients, are approximately constant in the considered spectral range, we find that the extremum values of the transmittance occur when the condition  $2\delta = j\pi; j = 0, 1, 2, \dots$  is satisfied. From this condition, the thickness of the film is given by  $d = \frac{j}{4\nu_j \sqrt{\hat{n}_s^2 - \sin^2 \phi_i}}$ , where  $\nu_j$  is the wavenumber corresponding to the extrema of order  $j$ .

However, this equation requires knowledge of the correspondence between the experimental extrema and the extremal order  $j$ , which often proves impractical. By considering two consecutive extrema, maxima or minima, we can dispense with this information and we arrive at Eq. 5, used for thickness calculations from the experimental spectra.

$$T = \frac{t_{as}^2 t_{sa}^2}{1 + r_{sa}^4 - 2r_{sa}^2 \cos(2\delta)}, \tag{4}$$

$$d = \frac{1}{4(\nu_{j+1} - \nu_j) \sqrt{\hat{n}_s^2 - \sin^2 \phi_i}}. \tag{5}$$

The wings of the *Episcada hymenaea* exhibit a notable level of homogeneity at visible wavelength scales, particularly within the bulk of the layer, comprising a composite of chitin, chitosan, and proteins as reported for the similar *Greta oto* species [19], also a member of the Ithomiini tribe [22]. Importantly, both chitin and chitosan exhibit minimal frequency dependence (low dispersion) of the refractive index within the spectral range under examination, while also displaying negligible absorption [23, 24]. Moreover, the anticipated anisotropy, which is effectively utilized in this technique, is expected to be exceedingly small. These combined factors render the utilization of Eq. 5 a reasonable approximation in this context.

### Results

For reference, the thickness of the sample was measured from the SEM image shown in Fig. 2a. Since the thickness exhibits variation across the wing, a total of 22 locations

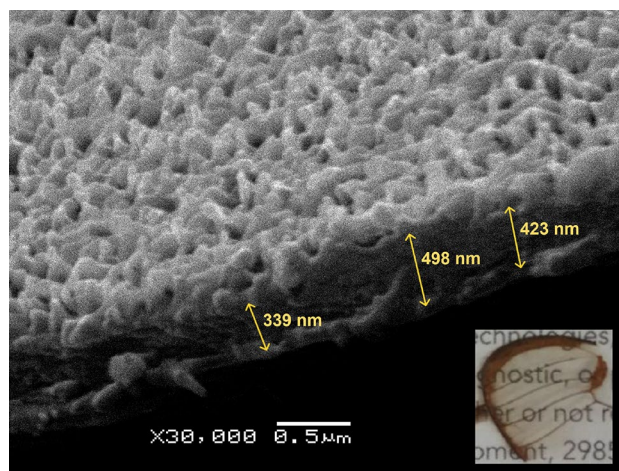
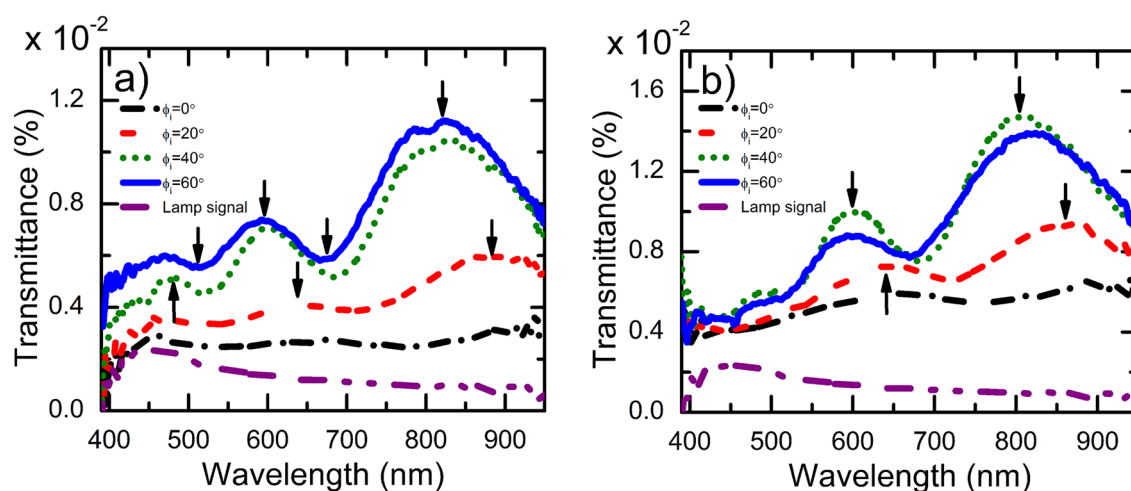


Fig. 2 SEM image of the side of the wing of a *Episcada hymenaea* butterfly specimen. For reference, three lengths across different regions are marked. In the insert, there is a picture of the wing



**Fig. 3** Transmittance spectra for the **a**  $T_{12}$  and **b**  $T_{21}$  configurations. As a visual aid, the arrows indicate the position of the extrema used in the thickness calculation

were sampled for analysis, with three of these locations highlighted in the provided image. To obtain an approximate value for the thickness, the average measurement was computed, while the standard deviation was employed as the associated uncertainty. A thickness of  $\bar{d} = 446 \pm 45$  nm was obtained.

The transmittance spectra for both crossed configurations are presented in Fig. 3. Notably, distinct interference oscillations are observed, which are absent in the lamp reference signal (Fig. 3) and the parallel transmittance spectra of the wing (Online Resource). From the maxima and minima within the spectra, Eq. 5 is employed to calculate the thickness of the wing. The average thickness and its associated uncertainty were determined using the mean and standard deviation, respectively.

A crucial factor to consider in the calculation is the refractive index of the sample. While the precise value remains unknown in this study, a commonly reported refractive index of 1.56 [23, 24] for chitin was employed as an initial reference. To explore the robustness of this technique to differences in refractive indices and obtain a range of thickness values, two additional values were considered. An index of 1.62, which closely aligns with the maximum reported value for chitin within the spectral range [23], was utilized as the lower bound. Conversely, an upper bound was calculated using  $n_s = 1.51$ , a value approaching the lowest refractive index reported for chitosan, a material with a lower refractive index than chitin, within the experimental wavelength range [23]. The results of these calculations are presented in Table 1.

The results demonstrate that all calculated thickness values align closely with the measurement obtained from the SEM image. Notably, the average thickness, which considers the combined thickness values from both configurations,

**Table 1** Calculated thickness values obtained for the *Episcada hyme-naea* butterfly wing using various refractive indices

Bound	Upper	Middle	Lower
$n_s$	1.51	1.56	1.62
Thickness $T_{12}$ (nm)	$417 \pm 38$	$400 \pm 35$	$381 \pm 32$
Thickness $T_{21}$ (nm)	$439 \pm 4$	$422 \pm 2$	$403 \pm 1$
Average thickness (nm)	$423 \pm 34$	$406 \pm 32$	$387 \pm 29$

The presented values include measurements for each individual configuration, as well as an average that incorporates all extrema observed in both configurations. The reported values represent the average thicknesses derived from different extrema, with the associated uncertainty expressed as the standard deviation

exhibits a maximum relative difference of 13% and a minimum of 5%. This observation is particularly noteworthy considering the non-uniform nature of the wing's thickness and the fact that the transmittance measurements were conducted in proximity to the center, as opposed to the edge observed in the SEM image.

Clearly the thickness values obtained from the  $T_{21}$  configuration exhibit closer proximity to the reference thickness and display smaller deviations. This outcome can be attributed to the increased signal strength associated with this polarization configuration, which subsequently enhances the signal-to-noise ratio and improves the definition of the observed maxima and minima. However, it is important to note that due to the reduced number of extrema evident in the spectra (Fig. 3b), the averaging process encompasses fewer data points, potentially explaining the decreased standard deviation observed.

An additional intriguing aspect revealed by Fig. 3 is the increase in transmittance when the sample is positioned

between the polarizers, an effect that is further amplified by increasing the angle of incidence. This phenomenon suggests that the sample induces a rotation in the polarization direction of the incident light, resulting in an intensified projection of light in the orthogonal direction. A material that rotates the plane of polarization of linearly polarized light is said to be optically active [25]. Previous reports have shown optical activity in the wings of other butterfly species, alongside polarization conversion effects dependent on the angle of incidence [10–13].

## Discussion

The theoretical framework leading to Eq. 5 provides a simple and convenient optical technique to determine the thickness of a sample, assuming certain conditions such as homogeneity, linearity, negligible absorption, and minimal dispersion of the refractive index reasonably approximate the material under investigation. However, in the case of the *Episcada hymenaea* butterfly wing, these interference oscillations are not observed in the direct polarization measurements (Online Resource). This absence of oscillations can be attributed to the combination of the very small reflection coefficient and the optical activity present in the sample. These factors contribute to the overwhelming dominance of the first term in the summation presented in Eq. 1. The small coefficients cause the summation terms to drop off rapidly, while the optical activity induces a rotation in the polarization direction, which depends on the path traversed through the sample. Because the interference is proportional to the scalar product of the fields [26], the increased rotation of the multiply reflected beams further reduces the interference interaction.

Recent studies have reported optical activity in both chitin [27] and chitosan [28]. Moreover, numerous works have revealed the occurrence of polarization conversion effects originating from nanostructures present in the wings of different butterfly species [10–13]. The bristles or microhairs on the transparent portion of the wing (Online Resource) closely resemble the organized structures observed in those species. It is possible that these bristles contribute to the polarization rotation, as the incident light spot, measuring approximately 2 mm in diameter, interacts with several of them. Another article demonstrated interesting polarization-dependent transmittance in the transparent part of the wings of the *Chorinea sylphina* species [6], which lacks reticular structures in the bulk of its wing but is covered with scales akin to the bristles observed in our species. The exact nature of the optical activity in the *Episcada hymenaea* is currently being investigated, and at present is an open question whether it arises from metastructures, the configuration of the constituent molecules, or both.

By utilizing the crossed polarization configuration for transmittance measurements, we exploit the polarization conversion to unveil the desired oscillations. Since the first term in the field summation only involves a single pass through the sample, it is expected that its rotation will be minimal. Therefore, this term becomes negligible when measuring in the orthogonal direction, effectively truncating the initial terms in the series. This in turn enables the emergence of the interference oscillations necessary for the application of Eq. 5.

## Conclusion

Through the implementation of this technique, we successfully obtained thickness values that closely matched the measurements obtained from a SEM image. Even without precise knowledge of the exact refractive index, the maximum difference observed between the calculated thickness and the reference value was 13%. The relative robustness to small variations in the refractive index demonstrates that this technique is suitable for the precise measurement of the thickness or as an initial estimate in the iterative process commonly employed to determine optical constants [17].

It is anticipated that this technique can be extended to other highly transparent materials that show polarization conversion characteristics. In particular, those composed of chitin and chitosan, which are increasingly being utilized as sustainable materials [29, 30].

**Supplementary Information** The online version contains supplementary material available at <https://doi.org/10.1557/s43580-023-00614-1>.

**Acknowledgments** This work was partially supported by PEDECIBA (Programa de Desarrollo de las Ciencias Básicas) - Física, ANII (Administración Nacional de Investigación e Innovación), and the CSIC (Comisión Sectorial de Investigación Científica) of the Universidad de la República, in Montevideo, Uruguay.

**Author contributions** JPM: Conceptualization, Methodology, data collection, formal analysis, Investigation, Writing—Original Draft, Writing—Review and Editing, Visualization. PF: Conceptualization, Validation, Writing—Review and Editing. CJP: Conceptualization, Validation, Methodology, Writing—Original Draft, Writing—Review and Editing. PV: Conceptualization, Validation, Methodology, Writing—Original Draft, Writing—Review and Editing. MP: Conceptualization, Validation, Writing—Review and Editing. GBV: Conceptualization, Sample preparation, Writing—Review and Editing. EM: Conceptualization, Sample preparation, Writing—Review and Editing. REM: Conceptualization, Methodology, Writing—Review and Editing, Supervision, Project administration.

**Funding** Agencia Nacional de Investigación e Innovación (ANII) (POS\_NAC\_2022\_1\_173968).

**Data availability** The data that support the findings of this study are available from the corresponding author, J.P. Martinez, upon reasonable request.

## Declarations

**Conflict of interest** The authors declare no conflict of interest regarding this article.

## References

1. Y. Wang, S.E. Naleway, B. Wang, Biological and bioinspired materials: structure leading to functional and mechanical performance. *Bioact. Mater.* **5**(4), 745–757 (2020). <https://doi.org/10.1016/j.bioactmat.2020.06.003>
2. K. Koch, B. Bhushan, Y.C. Jung, W. Barthlott, Fabrication of artificial Lotus leaves and significance of hierarchical structure for superhydrophobicity and low adhesion. *Soft Matter.* **5**(7), 1386 (2009). <https://doi.org/10.1039/b818940d>
3. B. Dean, B. Bhushan, Shark-skin surfaces for fluid-drag reduction in turbulent flow: a review. *Philos. Trans. R. Soc. A* **368**(1929), 4775–4806 (2010). <https://doi.org/10.1098/rsta.2010.0201>
4. R.Z. Wang, Z. Suo, A.G. Evans, N. Yao, I.A. Aksay, Deformation mechanisms in nacre. *J. Mater. Res.* **16**(9), 2485–2493 (2001). <https://doi.org/10.1557/JMR.2001.0340>
5. B. Bhushan, Y.C. Jung, K. Koch, Micro-, nano- and hierarchical structures for superhydrophobicity, self-cleaning and low adhesion. *Philos. Trans. R. Soc. A* **367**(1894), 1631–1672 (2009). <https://doi.org/10.1098/rsta.2009.0014>
6. N. Dushkina, S. Erten, A. Lakhtakia, Coloration and structure of the wings of *Chorinea sylphina* Bates. *J. Lepidopterists Soc.* **71**(1), 1–11 (2017). <https://doi.org/10.18473/lepi.v71i1.a2>
7. R. Li, S. Zhang, R. Zhang, Recent progress in artificial structural colors and their applications in fibers and textiles. *Chem.-Methods* **2**, e202200081 (2023). <https://doi.org/10.1002/cmtd.202200081>
8. S. Zhang, Y. Chen, Nanofabrication and coloration study of artificial Morpho butterfly wings with aligned lamellae layers. *Sci. Rep.* **5**(1), 16637 (2015). <https://doi.org/10.1038/srep16637>
9. S. Zobl, W. Salvenmoser, T. Schwerte, I.C. Gebeshuber, M. Schreiner, Morpho peleides butterfly wing imprints as structural colour stamp. *Bioinspiration Biomim.* **11**(1), 016006 (2016). <https://doi.org/10.1088/1748-3190/11/1/016006>
10. K. Zhang, Y. Tang, J. Meng, G. Wang, H. Zhou, T. Fan et al., Polarization-sensitive color in butterfly scales: polarization conversion from ridges with reflecting elements. *Opt. Express.* **22**(22), 27437 (2014). <https://doi.org/10.1364/OE.22.027437>
11. F. Liu, G. Wang, L. Jiang, B. Dong, Structural coloration and optical effects in the wings of *Papilio peranthus*. *J. Opt.* **12**(6), 065301 (2010). <https://doi.org/10.1088/2040-8978/12/6/065301>
12. D.G. Stavenga, M.A. Giraldo, H.L. Leertouwer, Butterfly wing colors: glass scales of *Graphium sarpedon* cause polarized iridescence and enhance blue/green pigment coloration of the wing membrane. *J. Exp. Biol.* **213**(10), 1731–1739 (2010). <https://doi.org/10.1242/jeb.041434>
13. D.G. Stavenga, The wing scales of the mother-of-pearl butterfly, *Protogoniomorpha parhassus*, are thin film reflectors causing strong iridescence and polarization. *J. Exp. Biol.* **224**, jeb242983 (2021)
14. R.A. Potyrailo, H. Ghiradella, A. Vertiatchikh, K. Dovidenko, J.R. Cournoyer, E. Olson, Morpho butterfly wing scales demonstrate highly selective vapour response. *Nat. Photon.* **1**(2), 123–128 (2007). <https://doi.org/10.1038/nphoton.2007.2>
15. M.I. Osotsi, W. Zhang, I. Zada, J. Gu, Q. Liu, D. Zhang, Butterfly wing architectures inspire sensor and energy applications. *Nati. Sci. Rev.* **8**(3), 107 (2021). <https://doi.org/10.1093/nsr/nwaa107>
16. N.L. Garrett, R. Sekine, M.W.A. Dixon, L. Tilley, K.R. Bambery, B.R. Wood, Bio-sensing with butterfly wings: naturally occurring nano-structures for SERS-based malaria parasite detection. *Phys. Chem. Chem. Phys.* **17**(33), 21164–21168 (2015)
17. H.G. Tompkins, J.N. Hilfiker, Optical data analysis. In: *Spectroscopic Ellipsometry: Practical Application to Thin Film Characterization*. 1st ed. Momentum Press; pp. 89–92. Google-Books-ID: Cj81CwAAQBAJ (2015)
18. J. Kim, K. Kim, H.J. Park, Thickness measurement of a transparent thin film using phase change in white-light phase-shift interferometry. *Curr. Opt. Photonics.* **1**(5), 505–513 (2017). <https://doi.org/10.3807/COPP.2017.1.5.505>
19. V.R. Binetti, J.D. Schiffman, O.D. Leaffer, J.E. Spanier, C.L. Schauer, The natural transparency and piezoelectric response of the Greta oto butterfly wing. *Integr. Biol.* **1**(4), 324 (2009). <https://doi.org/10.1039/b820205b>
20. R.H. Siddique, G. Gomard, H. Hölscher, The role of random nanostructures for the omnidirectional anti-reflection properties of the Glasswing butterfly. *Nat. Commun.* **6**(1), 6909 (2015). <https://doi.org/10.1038/ncomms7909>
21. O. Stenzel, The physics of thin film optical spectra: an introduction, in *Thick Slabs and Thin Films*. ed. by O. Stenzel. Springer Series in Surface Sciences. (Springer International Publishing, Cham, 2016), pp.131–161. [https://doi.org/10.1007/978-3-319-21602-7\\_7](https://doi.org/10.1007/978-3-319-21602-7_7)
22. R. Quinteros, E. Núñez Bustos, A Huge Aggregation of Episcada hymenaea (Lepidoptera: Nymphalidae: Danainae) in the Yungas of Northern Salta, Argentina. *Acta Zoológica Lilloana* **62**(2), 44–50 (2018)
23. D.E. Azofeifa, H.J. Arguedas, W.E. Vargas, Optical properties of chitin and chitosan biopolymers with application to structural color analysis. *Opt. Mater.* **35**(2), 175–183 (2012). <https://doi.org/10.1016/j.optmat.2012.07.024>
24. H.L. Leertouwe, B.D. Wilts, D.G. Stavenga, Refractive index and dispersion of butterfly chitin and bird keratin measured by polarizing interference microscopy. *Opt. Express* **19**(24), 24061–24066 (2011). <https://doi.org/10.1364/OE.19.024061>
25. X. Wang, Y. Yan, Optical activity of solids from first principles. *Phys. Rev. B* **107**(4), 045201 (2023). <https://doi.org/10.1103/PhysRevB.107.045201>
26. E. Hecht, *Interference*. In: *Optics*. 5th ed. Pearson Education, Incorporated; pp. 385–438. Google-Books-ID: ZarLoQEACAAJ (2017)
27. E. Belamie, P. Davidson, M.M. Giraud-Guille, Structure and chirality of the nematic phase in  $\alpha$ -chitin suspensions. *J. Phys. Chem. B* **108**(39), 14991–15000 (2004). <https://doi.org/10.1021/jp048152u>
28. A.B. Shipovskaya, S.L. Shmakov, N.O. Gegel, Optical activity anisotropy of chitosan-based films. *Carbohydr. Polym.* **206**, 476–486 (2019). <https://doi.org/10.1016/j.carbpol.2018.11.026>
29. H. Amiri, M. Aghbashlo, M. Sharma, J. Gaffey, L. Manning, S.M. Moosavi Basri et al., Chitin and chitosan derived from crustacean waste valorization streams can support food systems and the UN Sustainable Development Goals. *Nat. Food.* **3**(10), 822–828 (2022). <https://doi.org/10.1038/s43016-022-00591-y>
30. J. Hou, B.E. Aydemir, A.G. Dumanli, J. Hou, B.E. Aydemir, A.G. Dumanli. Understanding the structural diversity of chitins

as a versatile biomaterial. *Philos. Trans. R. Soc. A* **379**(2206), 20200331 (2021). <https://doi.org/10.1098/rsta.2020.0331>

**Publisher's Note** Springer Nature remains neutral with regard to jurisdictional claims in published maps and institutional affiliations.

Springer Nature or its licensor (e.g. a society or other partner) holds exclusive rights to this article under a publishing agreement with the author(s) or other rightsholder(s); author self-archiving of the accepted manuscript version of this article is solely governed by the terms of such publishing agreement and applicable law.